

Modelling Turbulence Using Vortex with Varying Strain Rate

Jun-De Li

School of Architectural, Civil, and Mechanical Engineering
 Victoria University of Technology, PO Box 14428, MCMC, Melbourne, 8001, AUSTRALIA

Abstract

In the last three decades, the study of turbulence, one of the great unsolved problems of classical physics, based on the dynamics of vortices and vortex motions has received continuing attention by physicists, engineers, and mathematicians. Here the solutions of Navier-Stokes (N-S) equations are used to show the dynamical behaviour of Lagrangian particles on the invariant plane of Velocity Gradient Tensors (VGT) for vortex with unsteady rate of strain. The results show that, for particles not too far from the vortex centre, the VGT invariant follows trajectories spiralling in towards the origin of the invariant plane, and follow a shape closely resembling to the conditional average from Direct Numerical Simulation of isotropic turbulence. These vortices of unsteady strain rates offer an explanation on forward and backward energy transfer.

Introduction

Turbulence is an omnipresent phenomenon of Nature and our understanding of it is still limited after more than one hundred years of studies. It is accepted that turbulent energy is distributed among eddies of various sizes and turbulent flows consist of randomly orientated vortices. One mechanism for the generation and maintenance of these vortices and their energies is through the vortex stretching. In [1], spiral vortices of different stages of stretching were used to model the small scale isotropic turbulence and a $-5/3$ law for the energy spectrum was derived in the inertial range. From a physical point of view, stretching of spiral vortices at high Reynolds numbers offers a simple explanation of energy transfer from large scales to small scales (forward cascade) with negligible energy dissipation, an important characteristics for the inertial range of isotropic turbulence [2]. In [3] and [4], randomly stretched Burger and spiral vortices were used to calculate the longitudinal structure functions, and reasonable agreements with experimental and numerical results were found. In [5], higher moments of one-point velocity derivatives were calculated using stretched spiral vortices. For a review on vortex dynamics in turbulence, see [6].

In all these studies, the vortices were stretched along the axial direction and little consideration was given to unsteady strain rates, especially those vortices of negative strain rates (compression) in the axial direction. One problem with using stretched vortices to model turbulence is that it cannot explain the energy transfer from small scales to large scales (backward cascade) as the experimental results [7] have shown that backward cascade happens very common in turbulent flow field. The other problem is that when the dynamics of stretched vortices are studied in the VGT invariant plane, only straight lines in the second and fourth quadrants can be produced [8]. Results in [8] show that different vortex circulations and stretching rates only result in changing the slopes of the straight lines in the invariant plane, not their quadrants. On the other hand, DNS results [8] show that a large portion of the data in the scattered plot of the VGT invariants falls in the first and third quadrants. The results in [8] also show that the time evolution of the invariants for conditional Lagrangian samples moves between quadrants.

In this paper, the solution of the Navier-Stokes equation for a vortex under varying strain rate is discussed first. The trajectories of the Lagrangian particles on the invariant plane will then be presented.

Vortex with unsteady strain rate

As pointed in [9], the evolution of the VGT following a fluid particle is of primary importance in the understanding of kinematics and dynamics of turbulence. Owing to its Galilean invariance property, the VGT contains significant fluid mechanics information independent of a non-accelerating observer. The dynamical behaviour of the VGT is of fundamental importance because it governs the mechanism of vortex stretching which in turn contributes to the energy cascade process in turbulent flows. Here we consider the evolution of the VGT invariants from velocity field induced by vortices with unsteady strain rates. The vorticity distribution is assumed to have only the axial component $\omega(r, t)$ in the cylindrical coordinate system (r, θ, z) and is a function of time t . The velocity field associated with this vortex is $\mathbf{v}_w = (0, v_\theta(r, t), 0)$. The vortex is exposed to an external irrotational strain field given by $\mathbf{v}_e = (-a(t)r/2, 0, a(t)z)$ and the total velocity field is given as

$$\begin{aligned} u_r &= -a(t)r/2 \\ u_z &= a(t)z \\ u_\theta &= v_\theta(r, t) \end{aligned} \quad (1)$$

Here we have assumed that the strain rate $a(t)$ is a function of time.

Lundgren [1] derived from the N-S equations an analytical solution for the axial symmetrical vortices with unsteady strain rate as

$$\begin{aligned} \omega(r, t) &= \frac{R_\Gamma S(t)}{T(t)} \exp\left(-\frac{r^2 S(t)}{4vT(t)}\right) \\ S(t) &= \exp\left(\int_0^t a(t') dt'\right) \\ T(t) &= \int_0^t S(t') dt' \end{aligned} \quad (2)$$

where R_Γ is Reynolds number and is related to the circulation Γ of a vortex by $R_\Gamma = \Gamma / 4\pi\nu$, and ν is the kinematic viscosity of the fluid. This solution represents flows in which a balance exists between convection, diffusion, and stretching or compression of the vortex. For $a(t) = \sigma = \text{const.} > 0$, the vortices become

$$\omega(r, t) = \frac{R_\Gamma \sigma}{1 - \exp(-\sigma t)} \exp\left(-\frac{\sigma r^2}{4\nu[1 - \exp(-\sigma t)]}\right) \quad (3)$$

When $t \rightarrow \infty$, this tends to the Burger vortex with a radius $r_B = (4\nu/\sigma)^{1/2}$.

A supervising feature of solution (2) is that the strain rate $a(t)$ can be any function of time. To study the dynamical behaviour of the vortices with unsteady strain rate, we assume

$$a(t) = \sigma \sin(2\pi ft) \quad (4)$$

where σ is the magnitude of the external strain rate and f is the frequency. This will involve both vortex stretching when $a(t) > 0$ and vortex compression when $a(t) < 0$. In turbulent flow fields of high Reynolds number, it is expected that a vortex cannot be stretched indefinitely such that high vorticity remains with a group of fluid particles all the time. Soon or later, a vortex will be compressed so that the particles previously having high vorticity will experience a decrease in vorticity. Also, for homogeneous isotropic turbulence, the assemble average of the strain rates is zero. Thus it is believed that a strain rate such as (4) can model more closely the external strain field experienced by a vortex than that of a constant stretch rate, and thus the dynamics of the vortices can be simulated more closely by using (4) than that by using Burger vortices. In calculating the statistics of velocity field induced by vortices, constant stain rate may be sufficient since in this case only a snapshot of the velocity field is needed. At this snapshot, all the turbulent quantities are 'frozen'. However, in order to study the dynamics of velocity field and to model the forward and backward energy transfer between turbulence scales, unsteady strain field is necessary. The tangential velocity field associated with solution (2) is

$$v_\theta(r,t) = \frac{2\nu R_\Gamma}{r} \left[1 - \exp\left(-\frac{r^2 S}{4\nu T}\right) \right] \quad (5)$$

Here we follow Lagrangian particles on the unsteady vortex and investigate the evolution of the particles in terms of vorticity and invariants of the VGT. The first, second and third invariants of the VGT are defined [10] as $P_A = -A_{ii}$, $Q_A = -A_{ij}A_{ji}/2$ and $R_A = -A_{ij}A_{ik}A_{kj}/3$, respectively, for the VGT $A_{ij} = \partial u_i / \partial x_j$. For incompressible flows, $P_A = 0$. As according to [10], local flows are represented by points in the (Q_A, R_A) -plane where the rotation and strain dominated flows are separated by zero discriminate curve $D = Q_A^3 + 27R_A^2/4 = 0$. The local topology of the flows for $D > 0$ and $R_A < 0$ is classified as stable focus/saddle, for $D > 0$ and $R_A > 0$ it is unstable focus/saddle, for $D < 0$ and $R_A > 0$ it is unstable node/saddle/saddle, and for $D < 0$ and $R_A < 0$ it is stable node/saddle/saddle. For the total velocity field given by (1) and (5), these invariants can be expressed as

$$\begin{aligned} Q_A &= -\frac{3}{4}a^2 - \left(\frac{v_\theta}{r}\right)^2 + \frac{\omega v_\theta}{r} \\ R_A &= -a\left[\frac{a^2}{4} - \left(\frac{v_\theta}{r}\right)^2 + \frac{\omega v_\theta}{r}\right] \end{aligned} \quad (6)$$

Particle trajectories on the invariant plane

Figure 1 shows the tangential velocity and axial vorticity following a particle at $r_0 = 5$, $z_0 = 1.0$ and $\theta_0 = 0$ at $t = 0$ with $R_\Gamma = 100$, $\sigma = 4$ and $\nu = 0.5$, calculated using (2) and (5). The radial position of the particle changes with time and was determined from $dr/dt = u_r$. The trajectory of the particle follows a spiral around the axis of the vortex and moves in the positive z direction (because $z_0 > 0$). Because of the axial symmetry, the initial position for z_0 and θ_0 can be arbitrary in calculating the quantities shown in the following figures. For the given

conditions for the vortex, the radius of the steady state Burger vortex with $a = \sigma$ is $r_B = 1/\sqrt{2}$. For the strain rate given by (4) with $\sigma = 4$, this particle oscillates between $5 \leq r < 1.4$ sinusoidally (results not shown).

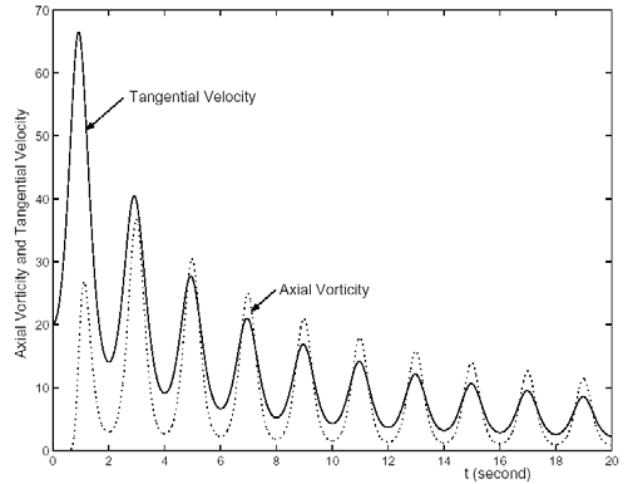


FIG 1. Axial vorticity and tangential velocity following a particle start at $r = 0$ with $R_\Gamma = 100$, $\sigma = 4$, $f = 0.5$ Hz and $\nu = 0.5$.

Figure 1 shows that at $t = 0$, the vorticity at the particle is zero and the tangential velocity $v_\theta = 2\nu R_\Gamma / r_0$. This can be explained by equations (2) and (5) which show that at $t = 0$, the vorticity is concentrated at $r = 0$ and singular. The tangential velocity at $r_0 = 5$ is that induced from a vortex line and thus the local flow field is irrotational. This singularity at $t = 0$ is not because of the unsteady strain rate (4) used. Equation (3) from a constant stretch rate also has this singularity. Of course, this singular vorticity would not exist in turbulence, at least for finite Reynolds numbers. This means that equations (2) and (5) cannot be used to model the onset of the Burger vortex.

Figure 1 also shows that the peak vorticity and the tangential velocity decrease with time. This is due to the characteristics of the stretch ratio $S(t)$ and vortex time $T(t)$ as defined in (2). Figure 2 shows the variations of $S(t)$ and $T(t)$ with time. It shows that the stretch ratio $S(t)$ oscillates but the vortex time $T(t)$ increases monotonically with no limit. Because of this, both the peak vorticity and tangential velocity decrease with time, and eventually approach zeros. This decrease of peak values for vorticity and tangential velocity with time is due to the continuous diffusion of vorticity away from the vortex centre with increasing vortex time $T(t)$. Another consequence of the monotonically increasing vortex time $T(t)$ and oscillating $S(t)$ is that the instantaneous vortex radius $r_s = (4\nu T(t)/S(t))^{1/2}$ as shown in figure 3 in general increases but oscillates with time. Figure 3 shows that as time increases, the region where the vorticity exists all the time increases as well. This spread of vorticity is due to the viscous diffusion.

Figure 4 shows the evolution of the given particle at $r_0 = 5$, $z_0 = 1.0$ and $\theta_0 = 0$ at $t = 0$ with $R_\Gamma = 100$, $\sigma = 4$, $f = 0.5$ Hz, and $\nu = 0.5$ in the invariant (Q_A, R_A) -plane. The second invariant Q_A has been normalized by

$Q_{A0} = \sigma^2 R_T / 4$ and the third invariant R_A has been normalized by $R_{A0} = \sigma^3 R_T / 4$. In figure 4, only the results from $4 \leq t \leq 60$ have been shown because of the singularity problem at $t = 0$ as discussed above. Also shown in the figure is the discriminate curve $D = 0$. It is found that at $t < 2$, the trajectory is below the $D = 0$. Equation (6) and the results in figure 1 show that the invariants are dominated by the flow field induced by the vortex as soon as the vorticity is above some threshold because of the relative large values of tangential velocity and vorticity in comparison with the strain rate.

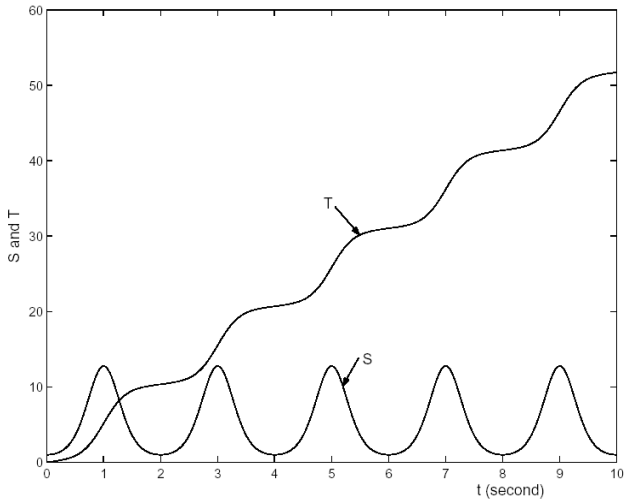


Figure 2 Stretch ratio $S(t)$ and vortex time $T(t)$ following a particle initially at $r = 5$ with $R_T = 100$, $\sigma = 4$, $f = 0.5$ Hz and $\nu = 0.5$.

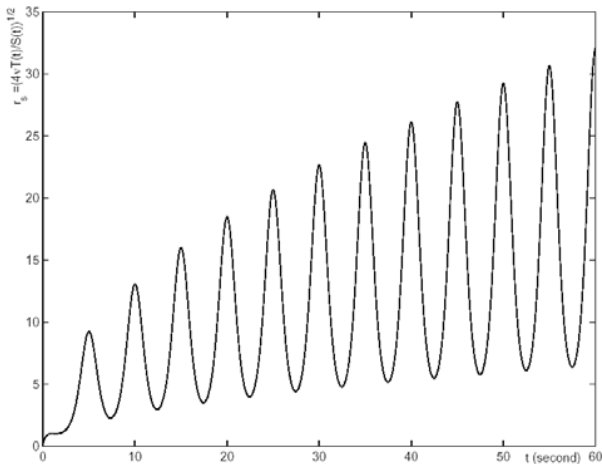


Figure 3 The instantaneous radius of the vortex with unsteady strain rate following a particle initially at $r = 5$ with $R_T = 100$, $\sigma = 4$, $f = 0.5$ Hz and $\nu = 0.5$.

It is found that for all the particles around the vortex, the trajectories of the invariants are similar to that shown in figure 4, each with a different time of moving above the $D = 0$ line. This trajectory shows two remarkable characteristics, i.e. it moves in the (Q_A, R_A) -plane in a clockwise fashion and it spirals towards the origin of the plane. These characteristics are the same as those shown by the conditional mean trajectories on the (Q_A, R_A) -plane given in [10] based on the DNS data of forced homogeneous isotropic turbulence. As the trajectory moves

towards the origin, the velocity gradient experienced by the particle decreases. The reason for this is that the peak vorticity and tangential velocity are decreasing with time as the results in figure 1 show.

Equation (6) shows that $R_A = 0$ at $a(t) = 0$. A close look at the results shows that the results for $R_A < 0$ corresponds to positive strain rate $a(t) > 0$ while those of $R_A > 0$ corresponds to negative strain rate $a(t) < 0$. Because it is generally believed that stretching vortex results in the energy transfer from large scales to small scales (forward cascade) and compressing vortex results in the energy transfer from small scales to large scales (backward cascade), then it can be concluded that the points on the left half of the (Q_A, R_A) -plane would involve forward cascade and those on the right half of the (Q_A, R_A) -plane would involve backward cascade. Using (6), it can also be easily shown that at any given time

$$R_A = -a(t)^3 - a(t)Q_A \quad (7)$$

This means that when $a(t) = \text{const.} > 0$, the trajectory would follow a straight line with a negative slope as the results in [8] show. Thus the spiral-in of the invariant trajectory shown in figure 3 is due to the variation of a strain rate $a(t)$ with time.

The results in Figure 3 should be compared with the solutions from the restricted Euler equations for the invariants [11]-[13],

$$\begin{aligned} \frac{DQ_A}{dt} &= -3R_A \\ \frac{DR_A}{dt} &= \frac{2}{3}Q_A^2 \end{aligned} \quad (8)$$

In (8), the pressure Hessian and the viscous term

$$H_{ij} = -\left(\frac{\partial^2 p}{\partial x_i \partial x_j} - \frac{\delta_{ij}}{3} \frac{\partial^2 p}{\partial x_l \partial x_l}\right) + \nu \frac{\partial^2 A_{ij}}{\partial x_l \partial x_l} \quad (9)$$

have been neglected. Figure 5 shows the solution of equation (8) in the invariant plane. In figure 5 the solution for the restricted Euler equation 'flows' from the left half of the plane to the right half of the plane and all solutions approach $D = 0$ as $t \rightarrow \infty$ rather than spiral in towards the origin of the invariant plane.

The reason for this difference in the invariant trajectory topology is that the results in figure 4 are based on the analytical solution of the N-S equations while those in figure 5 are based on the restricted Euler equations. Because of this, the effect of the pressure Hessian and the viscous term as given in (9) has not been neglected for the results in figure 4. This shows that correctly modelling the term in (9) is crucial in determining the invariant dynamics of the VGT. Numerical results in [14] show that the neglected pressure Hessian and the viscous term are at least as large as that due to convection.

Although isotropic turbulence consists of vortex of different scales and direction, each individual vortex may not last as long as the results given in figure 4. However, the results in figure 4 can be considered as a representative and ensemble of vortex at different stages of stretching and compressing from different vortices at different orientations. The results in figure 4 shows that this representative vortex can be used to study the statistics of turbulence. The strain rate given in (4) is of course too simple for a real turbulence. More complex forms of unsteady strain rate can be used to model the dynamic behaviour of the VGT invariants and make them to follow the DNS data more closely. The present results provide a starting point in building a realistic turbulence model.

Conclusions

The results presented here use solutions from the N-S equations and offer an explanation on the energy transfer mechanism

through both forward and backward cascades. The traditional understanding that energy transfer from large scale to small scale turbulence by a forward cascade process can only explain the energy transfer on average. The actual energy transfer mechanism involves forward and backward cascades. Any turbulence model and theory fail to include backward cascade cannot be expected to fully explain the nature of turbulence.

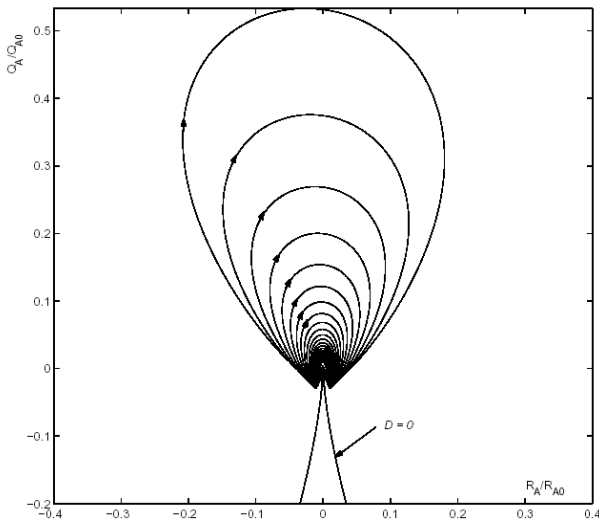


Figure 4 Evolution of invariants for a particle at $r_0 = 5$, $z_0 = 1.0$ and $\theta_0 = 0$ at $t = 0$ with the same conditions as those for figure 2.

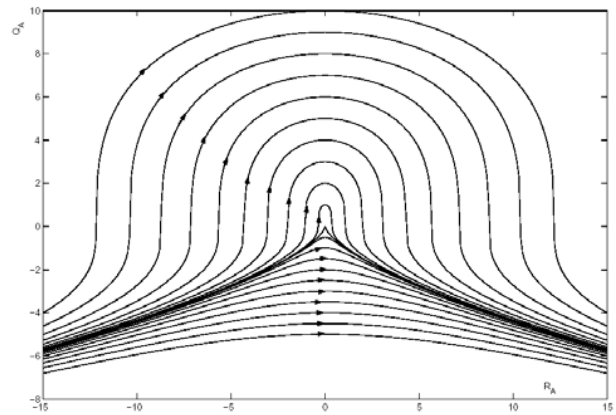


Figure 5 Solution to the Restricted Euler equation.

References

- [1] T. S. Lundgren, Phys. Fluid **25**(12), 2193 (1982).
- [2] U. Frisch, *Turbulence: The Legacy of A.N. Kolmogorov* (Cambridge University Press, Cambridge, England, 1995)
- [3] N. Hatakeyama and T. Kambe, Phys. Rev. Lett. **79**, 1257 (1997)
- [4] P.G. Saffman and D.I. Pullin, Phys Fluids **8**, 3072 (1996)
- [5] D.I. Pullin and P.G. Saffman, Phys. Fluids A **5**, 1787 (1993).
- [6] D. I. Pullin and P.G. Saffman, Annu. Rev. Fluid Mech. **30**, 31 (1998).
- [7] S. Liu, C. Meneveau and J. Katz, J. Fluid Mech. **275**, 83 (1994)
- [8] K. K. Normura and G.K. Post, J. Fluid Mech. **377**, 65 (1998).
- [9] Ooi, A., Martin, J. J. Soria and Chong, M., J. Fluid Mech. **381**, 141 (1998).
- [10] M.S. Chong, A.E. Perry, and B. J. Cantwell, Phys. Fluids A **2** (5), 765 (1990).
- [11] P. Viellefosse, J. Phys. Paris, **43**, 837 (1982).
- [12] P. Viellefosse, Physica A, **125**, 150 (1984).
- [13] B. J. Cantwell, Phys. Fluid A **4**, 782 (1992).
- [14] V. Borue and S. A. Orszag, J. Fluid Mech. **366**, 1 (1998).